Analyzing the Singularities of Freezing Sessile Water Droplets

Submitted in partial fulfillment of honors requirements
for the Department of Physics and Astronomy, Dickinson College,

by

Melia E. Bonomo

Advisor: Professor David P. Jackson
Advisor: Professor Trevor I. Smith

Reader: Professor Hans Pfister
Reader: Professor Lars Q. English
Reader: Professor Brett J. Pearson
Reader: Professor Catrina M. Hamilton-Drager
Reader: Professor Windsor A. Morgan

Carlisle, PA
May 13, 2013

Abstract

The purpose of this project is to investigate the singularity that forms at the tip of a water droplet freezing on a flat surface. By making several simplifications about the freezing process, we use a geometric model to derive a set of coupled differential equations that describe the volume, radius, and contact angle of the unfrozen liquid, and to describe the solidification rate.

We design an apparatus to observe 10-μL drops of purified water freezing on a chilled aluminum plate. A video camera is used to obtain a movie of the solidifying drop and capture the singularity that forms in the final moments. We then experiment with the use of dry ice as a cooling agent and perform video analysis to examine the changing dimensions of the liquid and solid portions of the drop during both methods of solidification.

We create a computer-based simulation that predicts the frozen droplet's shape, which is dependent on the density ratio of the solid to the liquid. We then use the simulation to produce a graphical animation of the shape transformation and to quantify the theoretical and experimental differences.

Analysis of our system of differential equations reveals the appearance of a pointy tip for liquids with a density ratio less than 0.75; this critical value is slightly higher in our simulation, at about 0.78. While the simplified model does predict the formation of singularities, it does not accurately predict the shape of frozen water droplets, which have an approximate density ratio of 0.9. We derive a second geometric model that accounts for a slightly curved solid-liquid contact line, which has been observed experimentally under certain initial conditions.

Acknowledgements

I would first like to thank all the people that have made this possible, especially my advisors Prof. Jackson and Prof. Smith, and my fellow group members Casey Caslin and David Lifschitz. I would also like to thank the entire Dickinson Department of Physics and Astronomy, for their constant support and enthusiastic encouragement. Special acknowledgements to Tonya Miller, Prof. English, and Rick Lindsey.

Contents

List of Figures

Glossary of symbols

A_s	cross-sectional area of solid
A_{sc}	cross-sectional area of spherical cap
α	angle within upside-down spherical cap (see Fig. 22)
β	free parameter controlling the curved solid-liquid interface evolution
Bo	Bond number
c	specific heat
F_γ	force of surface tension
F_g	force of gravity
g	force of gravity per unit mass, $9.81\,\mathrm{m/s^2}$
γ	force of surface tension per unit length
h	distance from center of sphere to base of spherical cap
k	thermal conductivity
κ	thermal diffusivity
L	length
L_f	latent heat of fusion
m_l	mass of liquid
m_s	mass of solid
ν	density ratio between solid and liquid
ϕ_i	growth angle between the tangents to the solid-vapor and liquid-vapor interfaces
Q	heat
$\vec{q}$	heat flux
R	base radius of liquid spherical cap
R_0	initial base radius of liquid spherical cap
$\mathcal{R}$	radius of full sphere of liquid spherical cap
$\mathcal{R}_c$	radius of full sphere of upside-down liquid spherical cap
$\mathscr{R}$	radius of perfect sphere at same volume as liquid spherical cap
ρ_l	density of liquid
ρ_s	density of solid
$\mathrm{d}s$	length of solid-vapor interface of newly frozen solid
t	time
T	temperature
T_c	temperature of cold surface under base of drop
T_f	freezing temperature of water

ΔT	temperature difference $T_f - T_c$
∇T	temperature gradient
$\mathrm{d}\tau$	thickness of newly frozen solid volume with curved solid-liquid interface
θ	contact angle of liquid spherical cap with surface beneath it
θ_0	initial contact angle of liquid spherical cap with surface beneath it
V_l	volume of liquid
V_{sc}	volume of spherical cap
V_s	volume of solid
z, z_f	height of solid layer, distance from cold surface to freezing front
$\mathrm{d}z$	thickness of newly frozen solid volume with flat solid-liquid interface
$\mathrm{d}z/\mathrm{d}t$	solidification rate
$z_{\max}$	final height of frozen drop, free parameter in our Curved Interface model

1 Introduction

A singularity is typically a location where a function (or its derivative) has an infinite or undefined value, around which a certain variable changes abruptly. Mathematically, this phenomenon can also occur at a singular point where the function is not "well-behaved," such as at a non-differentiable cusp. It turns out that, there are quite a few intriguing occurrences of these in nature [1]. For instance, we can see how the hair grows in various directions on each section of a baby's head, and the swirl of his cowlick is the point at which all of these differently oriented hairs meet. Similarly, the air is completely still in the eye of a hurricane, whereas there are strong winds blowing in every direction outside of this point. Or, more abstractly, consider what time it would be if we were standing in the very center of the North pole, the place at which all time zones converge; one might argue that it is "all times." Each of these examples reflects the system's attempt to confine opposing forces to a single point.

In fluid mechanics, we often see the emergence of singularities at the point between two fluid phases [2]. For example, sessile water droplets (immobile on a flat surface), that freeze from the bottom to the top, form a cusp at the very end of the transformation. This appears to be a result of the opposing forces of the liquid's surface tension and the solid's expansion while freezing, such that in the final moments of the solidification process, the liquid is forced to self-focus to a point. Though the increasing solid front moving up the height of the drop exhibits this pressure, surface tension in the remaining liquid portion tries to smooth out the cusp. Therefore, there is in fact a very slight curvature to the tip.

Studying the geometry of frozen water droplets is useful in understanding how ice accretions on wing surfaces will degrade aerodynamic performance, since it has been found that even the smallest change in texture has an effect on the forces created by the airfoil (wing shape) [3]. Stall warning systems are designed to activate based on the wing's angle of attack, and whether this inclination will cause too much drag or not enough lift for the aircraft. However, due to ice-accretions on the wing, drag increases more rapidly with an increasing angle of attack, which cannot necessarily be quantified within the warning system. Previous studies which simulated the effects of various droplet shapes and sizes have concluded that horn-shaped ice accretions have a greater impact on wing performance than smoother ice formations of a similar size. Therefore, the relationship between ice geometry and performance degradation can be used to design an airfoil that is less sensitive to icing, or even provide some method of quantifying the negative effects during flight.

Our research focuses on the case of just a single water droplet freezing on a cold surface. Using a simplified geometric approach, we aim to create a mathematical

description of this containerless solidification. We present a set of three differential equations that describe the liquid's changing volume, radius, and contact angle. By assuming a flat solid-liquid interface, we derive a fourth equation to describe the solidification rate. Analysis of these equations reveals the role that the density ratio ν (of the solid to the liquid) plays in the shape of the frozen drop. With this model, we expect to see pointy tips for liquids with a critical ratio of 0.75 or less.

Utilizing a high-resolution ProScope camera [4], we record solidifying water droplets in order to capture the cusp formation. We use two different freezing methods to observe the effects of different initial conditions. Analysis of these videos allows us to explore how the dimensions of the drop change during the freezing process.

We use Easy Java Simulations (*Ejs*) [5] with the above mentioned equations to create a computer program that generates predictions of frozen droplet shapes, based on various initial conditions, and produces a real-time animation of the solidification. The program successfully simulates the appearance of singularities for fluids that have a density ratio less than 0.78.

Considering that water has a density ratio of about 0.9, we quantitatively compare the differences between our experimentally-observed pointy droplets and the insufficient results of our model. Based on previous research findings [6], we derive a second geometric model that looks at the possibility of a curved solid-liquid interface. Experimentally, we attempt to gather evidence for or against this characteristic of solidification.

This paper explains the derivations of our two geometric models, the design and implementation of our experimental setup, and an analysis of our observed and simulated results. We believe that the inaccuracy of our theoretical approach is due to one or more of the simplifications we assume in order to derive our equations; the inclusion of these extra parameters is discussed as a possibility for further research.

2 Theory

To describe the theory behind sessile droplet solidification, we use a simplified geometric model that assumes the unfrozen liquid is a spherical cap shape, the slope between the solid and liquid layers is equal, and the solid-liquid interface is flat (as shown in Fig. 1) [2].

If we consider very small liquid droplets, we can neglect the effects of gravity according to the Bond number Bo [2]. This is a dimensionless ratio that tells us whether the force of gravity or the force of surface tension is more dominant in a liquid sessile drop of density ρ_l and volume V_l. We derive this relationship by looking

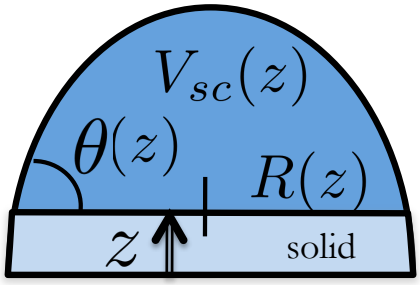

Figure 1: The unfrozen liquid is in the shape of a spherical cap with a volume V, radius R, and contact angle θ that depend on z, the height of the solid-liquid contact line.

at the gravitational force F_g per unit volume V_l within the liquid droplet

$$\frac{F_g}{V_l} = \rho_l g, \tag{1}$$

where g is the force per unit mass of gravity, and the force of surface tension F_γ over a certain length L

$$\frac{F_\gamma}{L} = \gamma, \tag{2}$$

where γ is the force per unit length of surface tension. To make these two equations dimensionally equivalent, we divide both sides of Eq. (2) by $\mathscr{R}^2$, where $\mathscr{R}$ is the radius of a perfect sphere with the same liquid volume as the sessile droplet

$$V_l = \frac{4}{3}\pi\mathscr{R}^3. \tag{3}$$

We create a dimensionless ratio between the force densities

$$\frac{\rho_l g}{\gamma/\mathscr{R}^2}, \tag{4}$$

which yields the Bond number

$$Bo = \frac{\rho_l g \mathscr{R}^2}{\gamma}. \tag{5}$$

As can be seen from the ratio, a low Bond number means that the system is more affected by surface tension forces. For a ratio of about 0.4 (which is cited as being reasonable for neglecting gravity [2]), we calculate that we need water droplets with a volume of $10\,\mu$L.

2.1 Flat Interface model

The volume of a spherical cap can be obtained from looking at the cap in terms of a full sphere, as portrayed in Fig. 2. We look at a circular slice πr^2 with a thickness

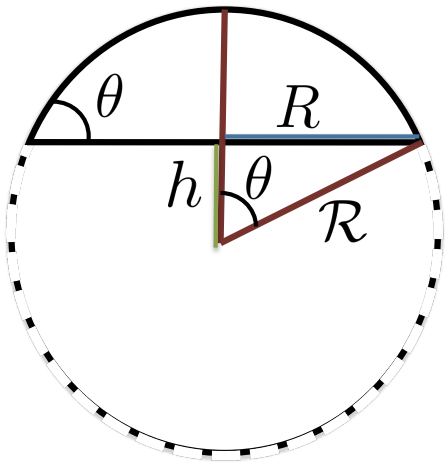

Figure 2: A diagram of our spherical cap in the context of a complete sphere, used to derive the liquid volume. Note, the base radius of our spherical cap is R, while $\mathcal{R}$ is the radius of the full sphere, and h is the height from the center of the sphere to the base of the cap.

$\mathrm{d}z$, where z is the height above the center of the sphere with radius $\mathcal{R}$, and r is the radial distance from the sphere's center at z, such that $r^2 = \mathcal{R}^2 - z^2$. We integrate this circular slice over the height of the spherical cap

$$V_{sc} = \int_h^{\mathcal{R}} \pi(\mathcal{R}^2 - z^2)\mathrm{d}z, \tag{6}$$

where $z = h$ and $z = \mathcal{R}$ are the distances from the center of the sphere to the base of the cap and the top of the sphere respectively, which yields

$$V_{sc} = \pi\left(\mathcal{R}^3 - \frac{1}{3}\mathcal{R}^3 - \mathcal{R}^2 h + \frac{1}{3}h^3\right). \tag{7}$$

We would like to eliminate h and $\mathcal{R}$ to create an equation for the volume that is only dependent on R and θ, the radius and contact angle at the base of the spherical cap. Using the relationships

$$R^2 = \mathcal{R}^2 - h^2 \tag{8}$$

$$h = \mathcal{R}\cos\theta \tag{9}$$

$$\mathcal{R} = \frac{R}{\sin\theta}, \tag{10}$$

as obtained from Fig. 2, we rewrite Eq. (7) and simplify. Our equation for the volume of a liquid spherical cap is therefore,

$$V_l = V_{sc} = \frac{\pi R^3}{3}\left(\frac{2 - 3\cos\theta + \cos^3\theta}{\sin^3\theta}\right), \tag{11}$$

where R is the base radius of the liquid droplet and θ is the contact angle between the liquid droplet and the surface beneath it [2].

We derive differential equations for the volume, radius, and contact angle of our shrinking liquid spherical cap with respect to small increases $\mathrm{d}z$ in the height of the solid layer as the droplet freezes, as seen in Fig. 1.

To describe how the liquid volume V_l decreases during solidification, we start with the idea of mass conservation,

$$-\frac{\mathrm{d}m_l}{\mathrm{d}t} = \frac{\mathrm{d}m_s}{\mathrm{d}t}, \tag{12}$$

where the mass of the liquid m_l decreases with time $\mathrm{d}t$ as the mass of the solid m_s increases. We write this equation in terms of the volume V and density ρ of the liquid and solid to get

$$-\frac{\mathrm{d}V_l}{\mathrm{d}t}\rho_l = \frac{\mathrm{d}V_s}{\mathrm{d}t}\rho_s. \tag{13}$$

Since we assume that the solid-liquid interface is flat, we describe the increasing solid volume $\mathrm{d}V_s$ as a circular slice πR^2 with thickness $\mathrm{d}z$, which leads to

$$-\frac{\mathrm{d}V_l}{\mathrm{d}t}\rho_l = \pi R^2 \frac{\mathrm{d}z}{\mathrm{d}t}\rho_s. \tag{14}$$

When we simplify and solve for $\mathrm{d}V_l/\mathrm{d}z$, we produce an equation describing how the volume of the liquid changes with respect to the freezing front height

$$\frac{\mathrm{d}V_l}{\mathrm{d}z} = -\nu\pi R^2, \tag{15}$$

where $\nu = \rho_s/\rho_l$ is the density ratio between the solid and the liquid [2].

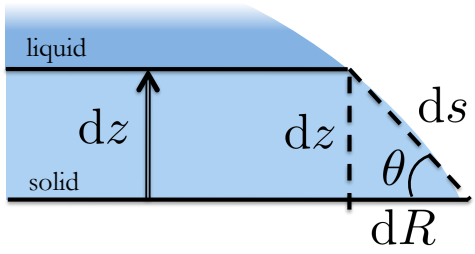

Figure 3: A close-up diagram of the increasing dV_s segment from Fig. 1. As the solid height dz increases, the radius dR of the liquid sphere cap shrinks, giving rise to Eq. (17). The increasing solid-vapor interface is given by ds.

We extract an equation to describe how the radius of the interface changes with height from examining the geometry of the solidification process. By zooming in on the newly formed $\mathrm{d}V_s$ slice, as seen in Fig. 3, we notice that the radius is shrinking

a distance of $\mathrm{d}R$ as the solid height increases $\mathrm{d}z$. Using the contact angle θ, we find the following relationship between the two parameters

$$\tan\theta = \frac{\mathrm{d}z/\mathrm{d}t}{-\mathrm{d}R/\mathrm{d}t}. \tag{16}$$

We then solve for $\mathrm{d}R/\mathrm{d}z$ to produce [2]

$$\frac{\mathrm{d}R}{\mathrm{d}z} = -\frac{1}{\tan\theta}. \tag{17}$$

Finally, to describe the changing contact angle of the liquid spherical cap as the drop solidifies, we differentiate Eq. (11) with respect to z to get

$$\frac{\mathrm{d}V_l}{\mathrm{d}z} = \frac{\partial V_l}{\partial R}\frac{\mathrm{d}R}{\mathrm{d}z} + \frac{\partial V_l}{\partial \theta}\frac{\mathrm{d}\theta}{\mathrm{d}z}. \tag{18}$$

We then use Eqs. (15) and (17), and solve for $\mathrm{d}\theta/\mathrm{d}z$, to come out with [2]

$$\frac{\mathrm{d}\theta}{\mathrm{d}z} = -\frac{1}{R}[\nu - (1-\nu)(2\cos\theta + \cos^2\theta)]. \tag{19}$$

A full derivation of this differential equation is described in Appendix A.1.

We describe the final size and shape of frozen droplets with Eqs. (17) and (19), which describe how the radius and contact angle respectively depend on the increasing height of the solid layer during containerless solidification.

2.2 Solidification rate

We derive an equation to describe the solidification rate of the droplet starting with Fourier's Law for heat conduction [7]

$$\vec{q} \propto -\nabla T, \tag{20}$$

which states that the heat flux $\vec{q}$ within the sold portion of the drop is proportional to the negative temperature gradient $-\nabla T$, the direction in which we have the greatest decrease in temperature. Equation (20) can be written as an equality

$$\vec{q} = -k\nabla T, \tag{21}$$

where k is the thermal conductivity of the material, and the heat flux is the small change in heat $\mathrm{d}Q$ in the time interval $\mathrm{d}t$ over the cross-sectional area A_s of the solid droplet. If we assume a one-dimensional temperature field in the z-direction within the solidifying drop, we can rewrite Fourier's Law as such

$$\frac{\mathrm{d}Q}{\mathrm{d}t}\frac{1}{A_s} = -k\frac{\mathrm{d}T}{\mathrm{d}z}. \tag{22}$$

We therefore also assume the change in temperature with respect to change in height will remain constant,

$$\frac{\mathrm{d}T}{\mathrm{d}z} = \frac{\Delta T}{\Delta z}. \tag{23}$$

The $\mathrm{d}Q/\mathrm{d}t$ in Eq. (22) refers to the flow of sensible heat

$$\mathrm{d}Q_{\text{sensible}} = c\Delta T \mathrm{d}m_s, \tag{24}$$

which is the small amount of heat released from the solid, according to its specific heat c, to lower the temperature of a small quantity of mass $\mathrm{d}m_s$ by ΔT (the temperature change of a slice that has a thickness Δz). Within each time step $\mathrm{d}t$, the solid portion of the droplet must be in a steady state, meaning the amount of heat that the solid releases must equal the amount of heat that it had absorbed. Considering our one-dimensional temperature field assumption, the heat that is released (as described by Eq. (24)) must have come from the heat that the solid absorbed from the liquid as it froze. This is the latent heat

$$\mathrm{d}Q_{\text{latent}} = L_f \mathrm{d}m_l, \tag{25}$$

which is the small amount of heat released from the liquid to perform the phase change of a small quantity of mass $\mathrm{d}m_l$ to a solid, according to the latent heat of fusion L_f of water. With heat and mass both conserved during solidification, we set Eqs. (24) and (25) equal to each other

$$-\frac{\mathrm{d}Q_{\text{sensible}}}{\mathrm{d}m_s} = \frac{\mathrm{d}Q_{\text{latent}}}{\mathrm{d}m_l}, \tag{26}$$

where, by convention, the amount of latent heat per small interval mass of the liquid that is absorbed by the solid is positive, and the amount of sensible heat per small interval mass of the solid that is released is negative.

After we plug Eq. (25) into Eq. (26), and solve for $\mathrm{d}Q_{\text{sensible}} = -L_f \mathrm{d}m_s$, we substitute this into Eq. (22),

$$\frac{-L_f \mathrm{d}m_s}{\mathrm{d}t A_s} = -k\frac{\Delta T}{z_f}, \tag{27}$$

where $\Delta T = T_f - T_c$ is the difference between the freezing temperature of the liquid T_f at the solid-liquid interface and the temperature of the cold surface T_c beneath the drop, and $\Delta z = z_f$, since it is the difference between the height of the freezing front z_f and the base of the drop $z_0 = 0$.

We manipulate this equation by multiplying the right hand side by $(c\rho_s/c\rho_s)$, where c is the specific heat of the solid and ρ_s is the ratio of the small amount of solid mass $\mathrm{d}m_s$ to its volume $\mathrm{d}V_s$. Furthermore, we substitute in the thermal diffusivity

$\kappa = k/c\rho_s$, which is a measure of how fast the heat is spreading with units of m^2/s, and the equation for the increasing solid volume in terms of the small change in height of the freezing front $\mathrm{d}V_s = A_s \mathrm{d}z_f$ (as stated in Eq. (14))

$$\begin{aligned} \frac{L_f \mathrm{d}m_s}{\mathrm{d}t A_s} &= c\frac{k}{c\rho_s}\frac{\mathrm{d}m_s}{\mathrm{d}V_s}\frac{\Delta T}{z_f} \\ &= c\kappa\frac{\mathrm{d}m_s}{A_s \mathrm{d}z_f}\frac{\Delta T}{z_f}. \end{aligned} \tag{28}$$

After simplifying, we rearrange the equation to create a separated differential equation

$$z_f \mathrm{d}z_f = \frac{c\kappa\Delta T}{L_f}\mathrm{d}t, \tag{29}$$

which we integrate from an initial solid height $z_f = 0$ at time 0, to a height $z_f = z$ at time t. When we solve the result for z

$$z = \sqrt{\frac{2c\kappa\Delta T}{L_f}t}\ , \tag{30}$$

we end up with an equation that describes the height of the solid layer $z(t)$ at any given time [8]. The derivative of Eq. (30) with respect to time

$$\frac{\mathrm{d}z}{\mathrm{d}t} = \sqrt{\frac{c\kappa\Delta T}{2L_f t}} \tag{31}$$

gives rise to an equation to describe the solidification rate.

We return to the derivations of the equations that describe the changing radius and contact angle according to the height of the solid, Eqs. (17) and (19) respectively, and put these in terms of $\mathrm{d}t$

$$\frac{\mathrm{d}R}{\mathrm{d}t} = -\frac{1}{\tan\theta}\frac{\mathrm{d}z}{\mathrm{d}t} \tag{32}$$

$$\frac{\mathrm{d}\theta}{\mathrm{d}t} = -\frac{1}{R}[\nu - (1-\nu)(2\cos\theta + \cos^2\theta)]\frac{\mathrm{d}z}{\mathrm{d}t}. \tag{33}$$

We now use Eqs. (32), (33), and (31) to predict the frozen droplet shape according to the rate at which the drops freeze.

2.3 Analyzing the differential equations

2.3.1 Frozen droplet profile

We combine Eqs. (32) and (33) to create a separable differential equation, which we can use to mathematically analyze the shape of the frozen drop at various density

ratios. We start by solving both equations for $\mathrm{d}z$

$$\mathrm{d}z = -\mathrm{d}R\tan\theta \tag{34}$$

$$\mathrm{d}z = -\frac{R\mathrm{d}\theta}{\nu - (1-\nu)(2\cos\theta + \cos^2\theta)}, \tag{35}$$

setting them equal to each other, and separating the R and θ variables to get [2]

$$\frac{\mathrm{d}R}{R} = \frac{\mathrm{d}\theta}{\tan\theta[\nu - (1-\nu)(2\cos\theta + \cos^2\theta)]}. \tag{36}$$

While it is possible to integrate this equation with any value of ν, one of the least complicated cases is when the solid and liquid densities are equal. Using $\nu = 1$ in Eq. (36) yields

$$\frac{\mathrm{d}R}{R} = \frac{\mathrm{d}\theta}{\tan\theta}. \tag{37}$$

We integrate each side with respect to its appropriate variable, from the initial radius R_0 and initial contact angle θ_0 to a current R and θ. The result is

$$R = \frac{R_0\sin\theta}{\sin\theta_0}, \tag{38}$$

which is a solution that corresponds to a perfect sphere with a radius $R_0/\sin\theta_0$ [2], as seen from Fig. 2 and Eq. (10). This makes sense because if there is no change between the liquid and solid densities, we would not expect to see a change in the liquid spherical cap's shape after solidification.

2.3.2 Final contact angle

To look at the possible solutions for the final contact angle, we need a differential equation that describes $\mathrm{d}\theta$ according to both the shrinking radius $\mathrm{d}R$ and the increasing solid height $\mathrm{d}z$. We create such a relationship by transforming Eq. (33) into an equation for $\mathrm{d}\theta/\mathrm{d}s$, where the changing solid-vapor interface $\mathrm{d}s$ (as seen in Fig. 3) is related to $\mathrm{d}z$ by

$$\mathrm{d}z = \sin\theta\,\mathrm{d}s, \tag{39}$$

where our new contact angle equation is therefore

$$\frac{\mathrm{d}\theta}{\mathrm{d}s} = -\frac{1}{R}\sin\theta[\nu - (1-\nu)(2\cos\theta + \cos^2\theta)]. \tag{40}$$

We determine the final contact angle when Eq. (40) equals zero, which gives us either

$$0 = \sin\theta \tag{41}$$

or

$$0 = \nu - (1-\nu)(2\cos\theta + \cos^2\theta). \tag{42}$$

Since θ is limited to $0 \leq \theta < \pi$, Eq. (41) leads to

$$\theta = 0, \tag{43}$$

which refers to a frozen drop with a flat top, and is a solution for all values of ν. Equation (42) can be written as

$$0 = \cos^2\theta(\nu - 1) + \cos\theta(2\nu - 2) + \nu, \tag{44}$$

which we solve using the quadratic formula and simplify to

$$\cos\theta = \pm\frac{1}{\sqrt{1-\nu}} - 1. \tag{45}$$

After checking both solutions, we find that only the positive sign satisfies Eq. (40), and we see that the contact angle at the top of the frozen drop depends only on ν via

$$\theta = \cos^{-1}\left(\frac{1}{\sqrt{1-\nu}} - 1\right). \tag{46}$$

Because the limit of the cosine function is ± 1, substituting $\cos\theta = 1$ into Eq. (46) reveals that a solution does not exist for $\nu > 0.75$.

When we graph Eqs. (43) and (46), as shown in Fig. 4, we see the presence of this critical value of ν causing a pitchfork bifurcation. A bifurcation occurs when a small smooth change made to a parameter (in this case ν) causes a sudden qualitative change in the system's behavior. When $\nu < 0.75$, we expect to see a pointy solidified drop because Eq. (46) is the stable solution. However, for $\nu > 0.75$, Eq. (46) has no solution, and we are left with flat-topped solidified drops based on Eq. (43).

We can prove that Eq. (43) is unstable for $\nu < 0.75$ by thinking of Eq. (40) as a function of θ

$$f(\theta) = -\frac{1}{R}\sin\theta[\nu - (1-\nu)(2\cos\theta + \cos^2\theta)] \tag{47}$$

and analyzing the derivative of this function at $\theta = 0$ [9]. Figure 5 graphs $f(\theta)$ for small changes in the contact angle, near the end of solidification. For all ν values, the function equals zero at $\theta = 0$, however the derivatives are not the same. As $f(\theta)$ approaches zero at the end of solidification, we see that $f'(\theta) < 0$ for $\nu > 0.75$, meaning that the function is evolving towards the $\theta = 0$ solution. Whereas for $\nu < 0.75$ we see that $f'(\theta) > 0$, meaning the function evolves away from the solution $\theta = 0$, giving rise to the instability. When $\nu = 0.75$, $f'(\theta) = 0$ at/near $\theta = 0$. Therefore, we can cite $\nu = 0.75$ as the critical value at which the stability of the flat top solution changes. This analysis is useful because it allows us to see how the instability arises that leads to a pointy tip.

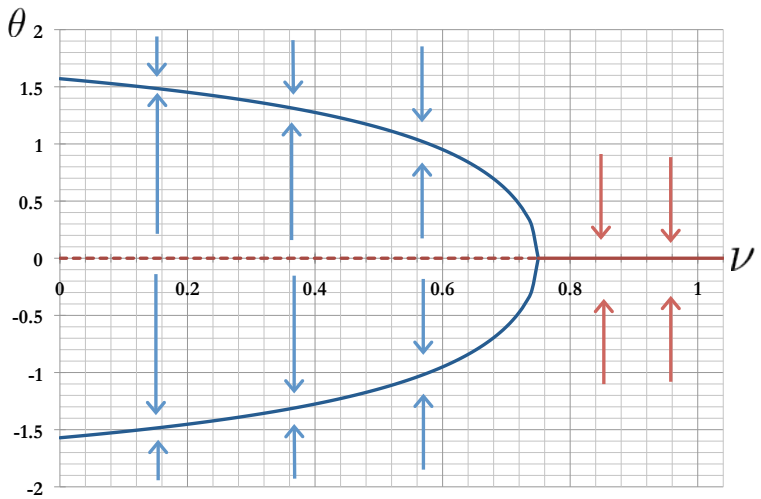

Figure 4: Graph of the final contact angle θ (in radians) versus the density ratio ν from Eq. (43) (red line) and Eq. (46) (blue line). The arrows indicate the direction in which the system evolves toward a stable solution (solid curves are stable; dashed are unstable). Note the appearance of a final non-zero contact angle only at density ratios of $\nu < 0.75$; for ratios higher than this critical value we see frozen drops with flat tops.

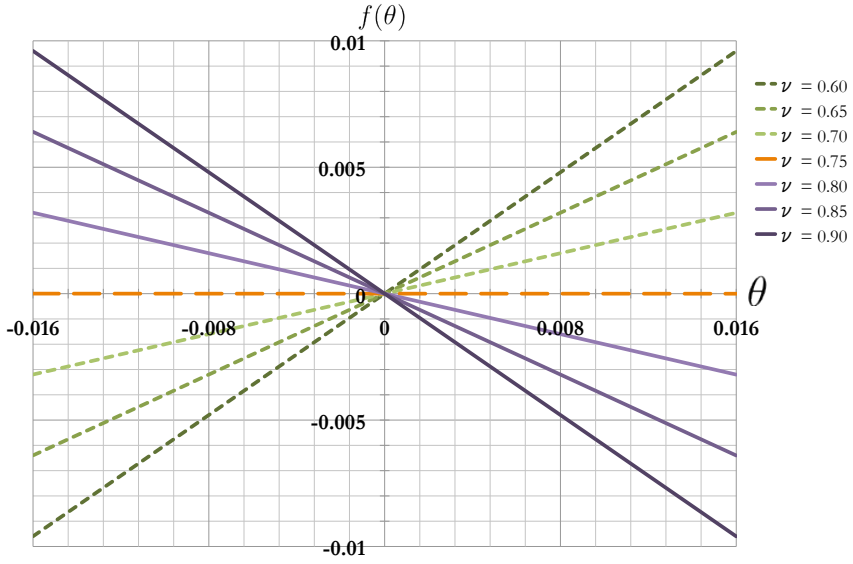

Figure 5: Graph of Eq. (47) for various density ratios ν, to analyze the stability of the solution $\theta = 0$, Eq. (43). Note that $\nu = 0.75$ is the critical value at which the stability of this solution changes. The dotted lines represent the values of ν for which the solution $\theta = 0$ is unstable, where $f'(\theta) > 0$, and the solid lines are the stable solutions, where $f'(\theta) < 0$.

3 Experimental Methods

The main experimental goals were to obtain a clear video of a freezing sessile water droplet in order to study the pointy tip that appeared and compare the solidification process to our geometric model. We observed solidifying droplets by means of two experimental setups: one in which we froze the drop on top of a chilled aluminum plate, and the second in which we froze the drop directly on dry ice.

In both setups we made use of a micropipette to obtain 10-μL drops of water. After setting the desired volume with the dial on the device, which has a range from $5\,\mu$L to $40\,\mu$L, we placed the tip into a beaker of purified water. This was colored with green food-dye to improve the video contrast. To dispense uniformly-sized droplets, we gently depressed the top button of the pipette until this pressure was met by a light resistance.

For both still-image and video capturing, we employ a ProScope HR [4]. This is a handheld USB microscope with high resolution capabilities. Specifically, the still-image resolution is 1280×1024 pixels, and the video resolution is 1280×1024 pixels at 3.75 frames per second. The lens had $50\times$ magnification strength and $0.5''$ focal length. We made sure that the ProScope HR was angled completely horizontal to the cold plate plane. The LED lighting option on the device provided sufficient illumination of the freezing droplet.

We also used a thermocouple with a low-temperature surface probe to record the temperature of the cold plate or dry ice during the drop's solidification. The probe head consisted of two coils soldered together, which make accurate temperature readings down to -250 °C. It connected to a thermocouple, which sent the temperature input to LoggerPro [10].

3.1 Freezing droplets on a metal plate

We first built an apparatus (as seen in Fig. 6) that consisted of a quarter inch-thick aluminum plate, which securely fit over the opening of a seamless polystyrene box. Our most efficient design for the base was an $8'' \times 9'' \times 2''$ solid box, with a $5.5'' \times 5.5'' \times 1.25''$ cavity removed. We carved a $0.25''$-wide lip around the top of the cavity for our $6'' \times 6'' \times 0.25''$ aluminum plate to rest on. Through a small cutout left for ventilation, we poured liquid nitrogen into the box to uniformly chill the plate. This was a $1''$ wide $\times$ $0.75''$ deep cutout made to give the liquid nitrogen an outlet for expelling vapor as it boils away. Liquid nitrogen is a colorless clear liquid which boils at 77 K (-196 °C) at atmospheric pressure. While the material is not highly dangerous, we took certain precautions when handling it, such as using special gloves.

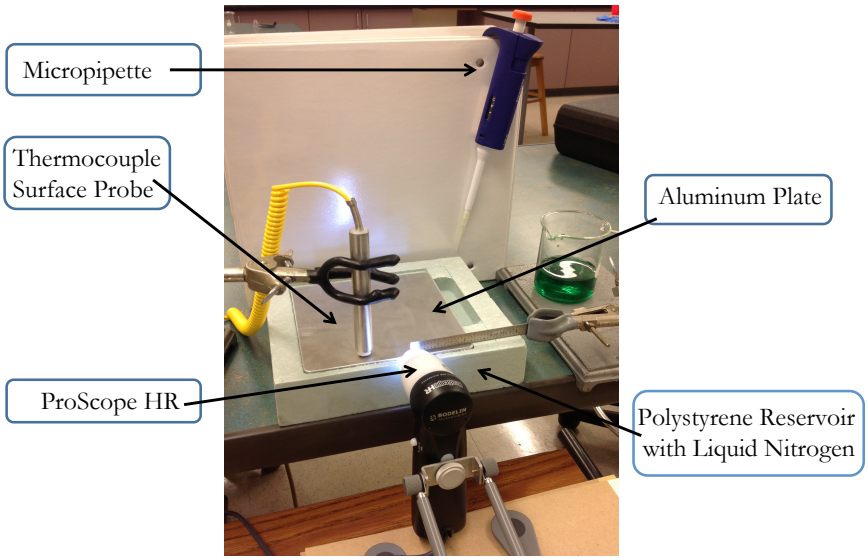

Figure 6: A photograph of our experimental setup for freezing water droplets on a metal surface. A micropipette produces 10-μL water drops onto an aluminum plate that is chilled from below by a reservoir of liquid Nitrogen. A ProScope HR video camera is used to record the freezing process, and a thermocouple surface probe is used to record the temperature of the plate.

The micropipette allowed us to place uniform drops of distilled water onto the aluminum plate. We used the ProScope to magnify and capture the freezing process, as seen in the progression of images shown in Fig. 7. By freezing drops at various plate temperatures (in small increments from about -20 °C to -40 °C), we were able to analyze the effect temperature difference has on the solidification process.

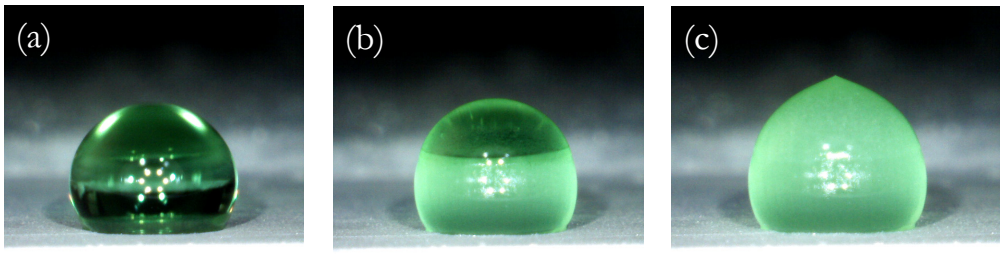

Figure 7: A succession of photographs taken by our ProScope HR to illustrate the freezing process: (a) the initial liquid water drop, (b) midway through solidification, and (c) the frozen drop with its pointy tip.

3.2 Freezing droplets on dry ice

We also froze water droplets directly onto dry ice, as shown in Fig. 8. We again made use of the micropipette for dispensing uniform drops, the ProScope for close-up video capture, and the thermocouple to check the temperature of the surface (which remained at about -70 °C). Special care had to be taken when dropping the liquid water onto dry ice because the drops often slipped off the side.

It is also important to note that when the room temperature liquid comes into contact with the dry ice, it melts some of the dry ice, causing the drop to sink down slightly. We speculate that this may change the physics of the situation, since the sides of the base of the water drop are now in contact with the dry ice. This phenomenon will be further discussed in Sec. 6.4.

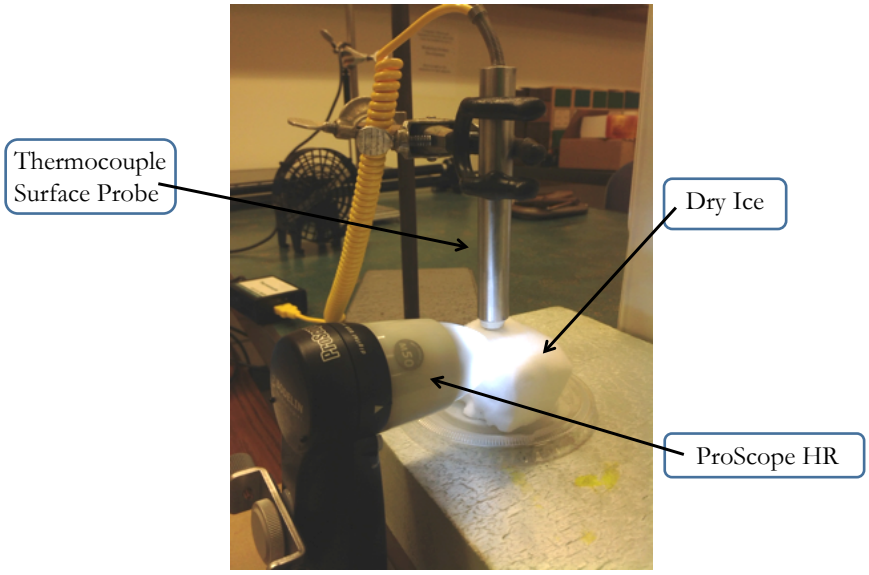

Figure 8: A picture of our experimental setup for freezing water droplets directly onto dry ice. A ProScope HR is used to record the freezing of 10-μL water droplets, and a thermocouple surface probe is used to record the temperature of the dry ice.

4 Results

4.1 Experimental observations

After assessing and adjusting the various parameters of the experiment (lighting, droplet size, camera resolution, etc.), we were able to obtain a clear movie of a solidifying water droplet on the aluminum plate using the ProScope. Initially, the

droplet sat on the plate in the shape of a spherical cap. Over a period of about $5-15\,\mathrm{s}$, the drop froze from the base upwards and remained rounded on top for most of this process. On dry ice, solidification occurred in the same fashion, typically in about $40\,\mathrm{s}$. It was not until the final moments of solidification that we observed the formation of the singularity; the pointy tip appeared to spontaneously pop up in the last second or so.

4.1.1 Analyzying the solidification rate

We performed video analysis using LoggerPro to examine the changing dimensions of the liquid and solid portions of the drop during solidification for droplets freezing on three different plate temperatures and on dry ice.

Based on the frame rate of our video file, we manually tracked the height of the freezing drop every $0.39\,\mathrm{s}$. For each video, we marked the evolution of the solid's vertical height fives times in order to calculate an average with appropriate error bars. In our dry ice video, the liquid drop initially sinks down, therefore we also tracked the average descent of the top of the drop. We then calculated the distance the drop sank at each time step and added this discrepancy to the solid height data.

We created a z versus t plot for drops freezing on the aluminum plate (as shown in Fig. 9). Also included are the theoretical $z(t)$ equations (dotted curves) calculated from Eq. (30) and the power functions $z = At^B$ calculated to fit each data set (solid curves). Figure 10 shows the height of the solid layer only in the first $3.2\,\mathrm{s}$ of solidification, which slightly changed the function of best fit. This time interval was chosen with trial and error, based on our attempt to demonstrate the data's $\sqrt{t}$ behavior predicted by our theoretical $z(t)$. It is interesting to note that our model fits best for the first $3.2\,\mathrm{s}$ of drops freezing on colder plate temperatures.

We then created a $\mathrm{d}z/\mathrm{d}t$ versus t plot (Fig. 11) from the values LoggerPro automatically calculated during video analysis for one of the droplets freezing on the aluminum plate. We included our theoretical expectation, (Eq. (31) plotted as a dotted curve), with a power function fit to the data (plotted as a solid curve). Again, we showed how the power function changes for isolating just the first $3.2\,\mathrm{s}$ of data (see Fig. 12). While the theoretical $\mathrm{d}z/\mathrm{d}t$ (or even the expectation of $1/\sqrt{t}$ behavior in general) does not fit as well as the $z(t)$ did for the same data set, we can see a trend in the decrease in solidification rate over time to a constant velocity. The rate picks up again, however, in the last second when the singularity appears.

Figure 13 shows $z(t)$ for the water droplet freezing on dry ice. With the $70\,\mathrm{K}$ difference between the dry ice and the water droplet, Eq. (30) predicts a much faster solidification time than what was experimentally observed and, contrary to our theory,

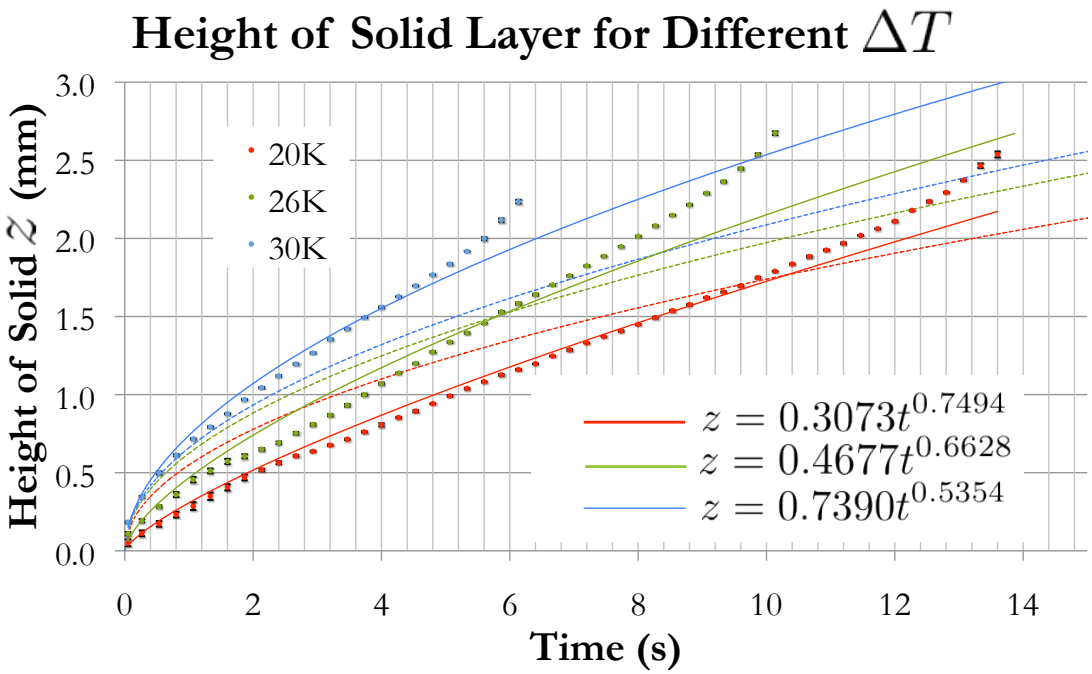

Figure 9: Graph of the change in vertical height of the solid layer with respect to time based on various ΔT. Experimental values were obtained from video analysis with LoggerPro, the dotted curves are our theoretical expectations calculated from Eq. (30), and the solid curves are trend lines obtained for the data.

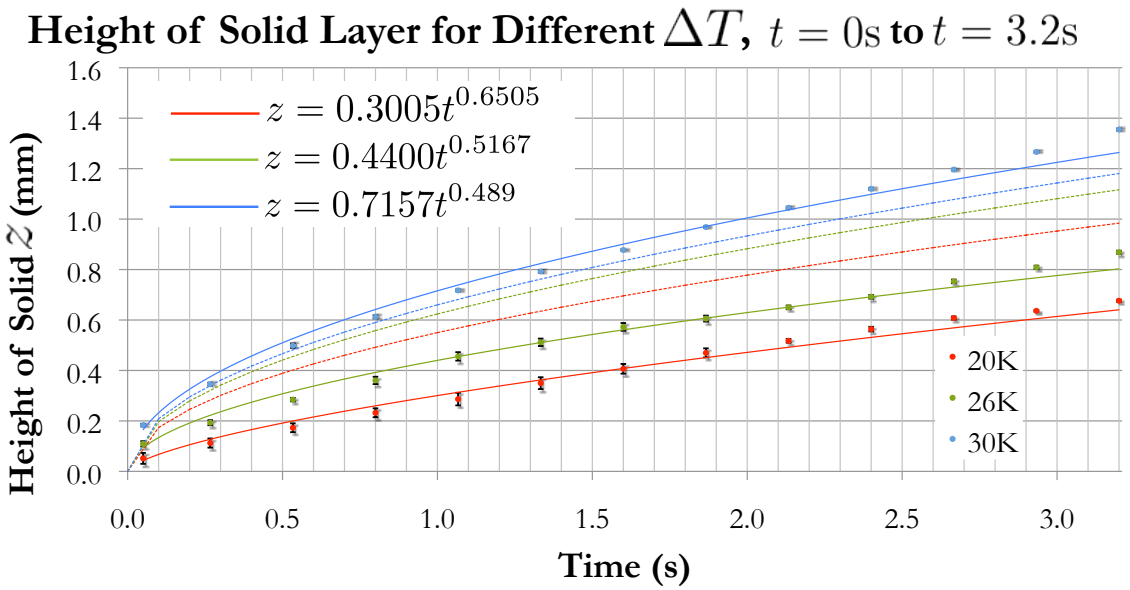

Figure 10: Graph of the change in vertical height of the solid layer with respect to time based on various ΔT for the first 3.2 s of solidification. Experimental values were obtained from video analysis with LoggerPro, the dotted curves are our theoretical expectations calculated from Eq. (30), and the solid curves are trend lines obtained for the data.

the experimental solidification rate appears to speed up over time.

4.1.2 Experimental issues

We did run into a few experimental issues along the way. The aluminum plate became so cold that it caused water vapor in the immediate vicinity to condense onto the plate. This first of all created a thin layer of frost that we would repeatedly have to clear off, to avoid changing the initial contact angle between the liquid and plate. There was also fog that interfered with our video capture, because the wafting movement caused the ProScope to have difficulty focusing on the drop. We somewhat solved this issue by using a small fan to blow the vapor away.

Additionally, while we tried to account for the sinking of the droplet on dry ice, it was still difficult to track the solid front in the beginning stages of solidification. This was mainly due to the presence of bubbles within the drop (from carbon dioxide being released as the room-temperature water droplet cause some of the dry ice to sublime) and water vapor around it.

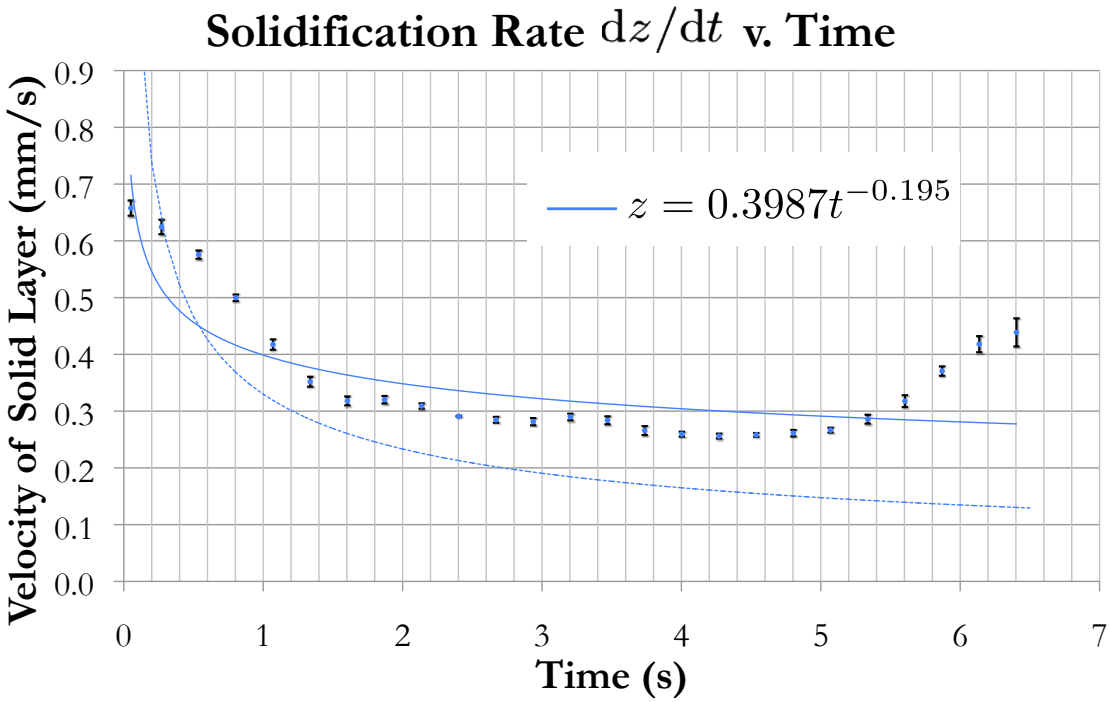

Figure 11: Graph of the solidification rate dz/dt with respect to time for $\Delta T = 30\,K$. The dotted curve is our theoretical Eq. (31), and the solid curve is a power function fit to the data.

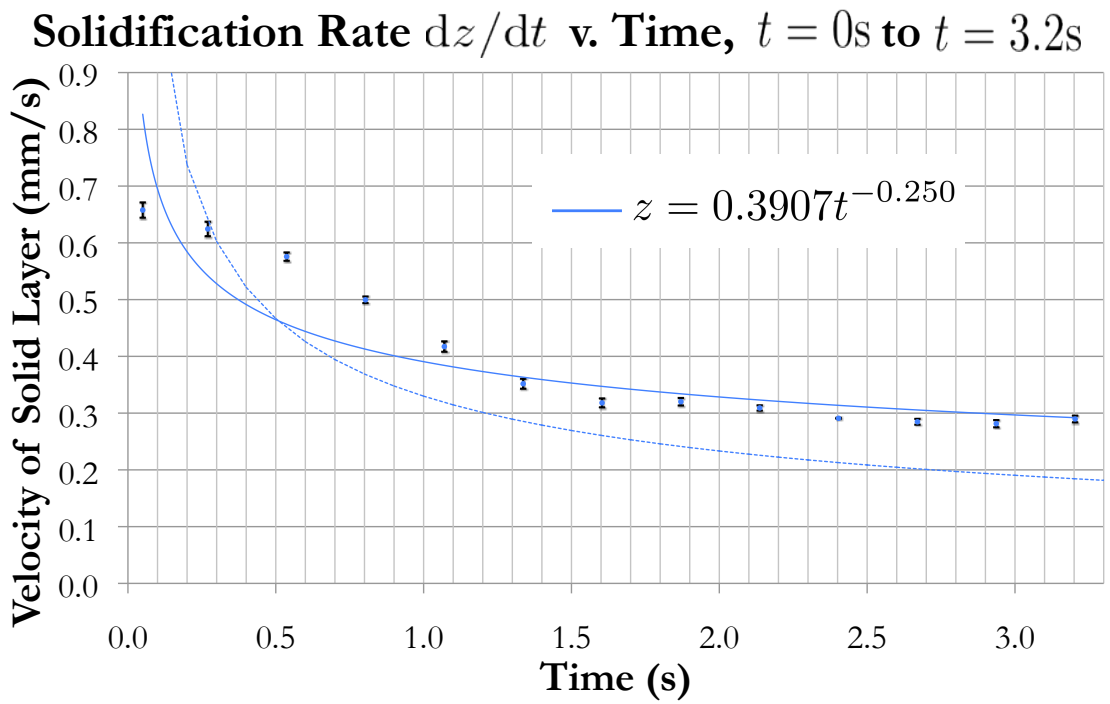

Figure 12: Graph of the solidification rate dz/dt with respect to time for $\Delta T = 30\,K$ during the first 3.2 s of freezing. The dotted curve is our theoretical Eq. (31), and the solid curve is a power function fit to the data.

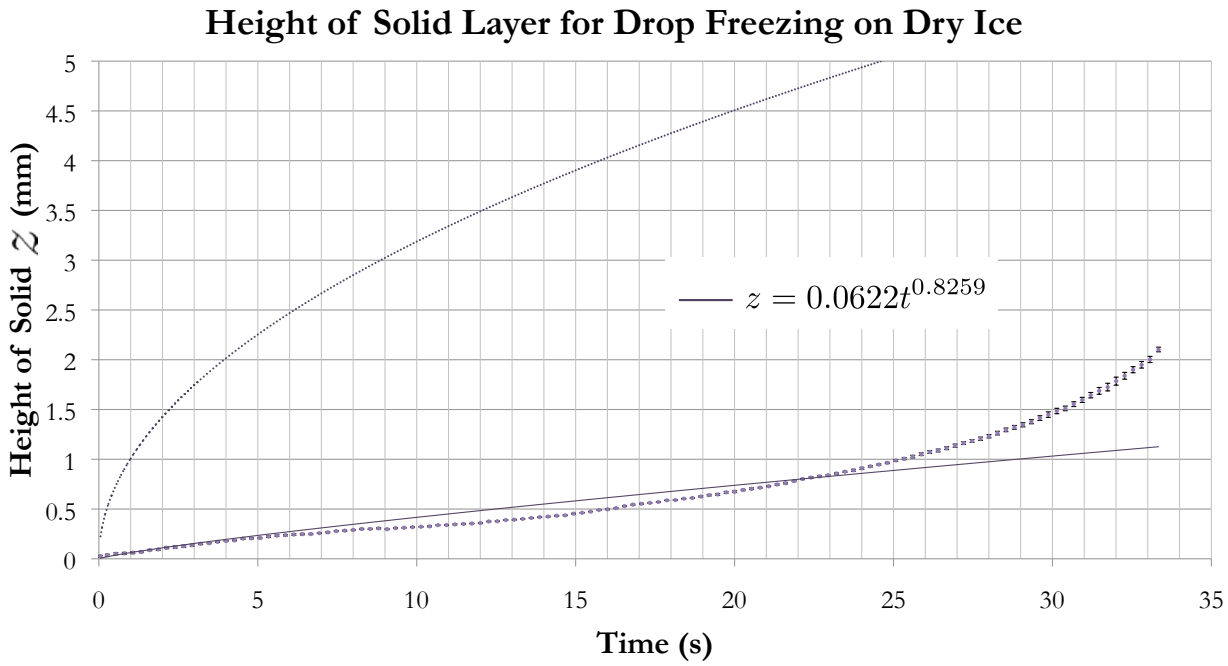

Figure 13: Graph of the solid height $z(t)$ of a droplet freezing directly on top of dry ice. The data points reflect our attempt at normalizing discrepancies caused by the drop sinking down into the dry ice during solidification. The solid curve is a power function that was fit to the data, and the dotted curve is calculated from our theoretical Eq. (30).

4.2 Numerical results

4.2.1 Predicting frozen droplet shapes

We modeled the final shape of freezing droplets with the solidification rate, radius, and contact angle differential equations (Eqs. (31), (32), and (33) respectively) using Easy Java Simulations (*Ejs*) [5] [11]. This programming tool allowed us to efficiently predict the appearance of a singularity at various density ratios. It provided a simplified method of simulating the phenomenon, and placed emphasis on the resulting Java program rather than the heavy programming that might otherwise have been needed to create it.

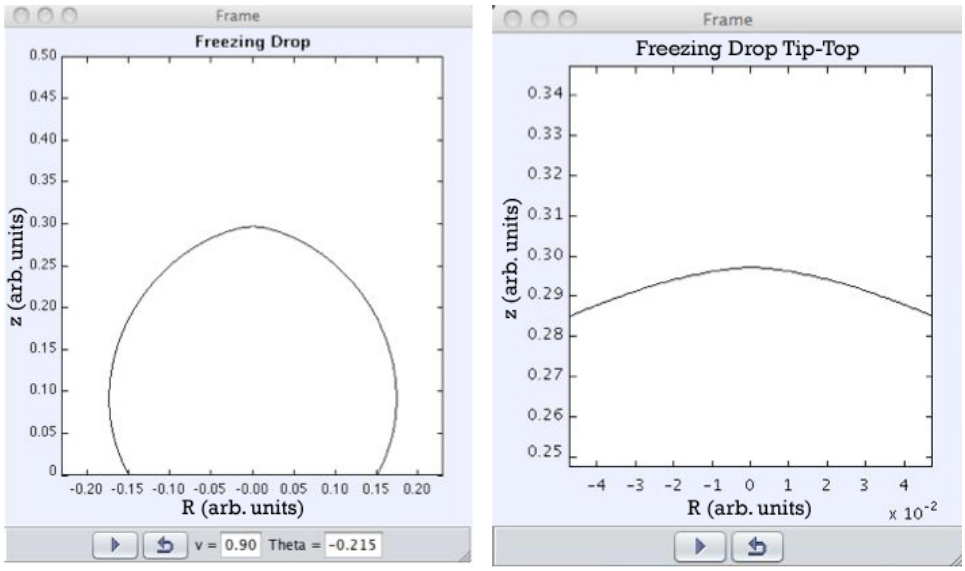

Figure 14: The output from our Ejs simulation for a frozen drop with a density ratio $\nu = 0.9$, initial contact angle $\theta_0 = 2.09\,rad$, and initial radius $R_0 = 0.15\,arb$ (left), with a close-up view of the droplet's tip (right).

After we defined our first-order differential equations with arbitrary values for the initial R and θ, we chose to solve our equations with the 4^{th}-order Runge-Kutta algorithm. We then used the drawable elements in *Ejs* to create a graphical representation of the results. Currently our simulation creates a z versus R plot of the solidified drop, with a second enlarged graph that focuses in on the drop's tip, (see Fig. 14).

With z as our independent variable, we set a small increment size for $\mathrm{d}z$ to obtain detailed information about the tip of the drop (the smaller the increment, the more accurate our results were). We also defined an event such that the program would stop running before R went to exactly zero, to avoid the zero denominator that would

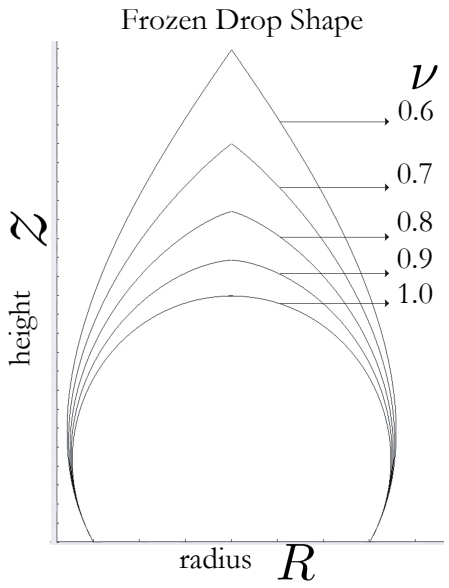

Figure 15: Simulations of various frozen drop shapes based on density ratios $\nu = 1.0$ *to* 0.6*, with* $\theta_0 = 2.09$ *rad and* $R_0 = 0.15$ *arb. The Ejs simulation shows how the conical tip becomes sharper as the density ratio decreases.*

result in Eq. (33). This condition did not have any negative effects on the final shape since our limit was on the order of 10^{-8}.

While ν is the only variable that remains constant during the running simulation, we designed the program such that we could easily restart it with different ν values to compare the differences in frozen drop shape. By plotting several solidified shapes on the same graph (see Fig. 15), we determined that as the density ratio decreased, the pointy tip became sharper.

We compared one of the experimental data sets from the droplet freezing on the chilled cold plate to our numerical results. Using the initial radius and contact angle obtained from video analysis, $R_0 = 1.5\,\text{mm}$ and $\theta_0 = 2.29\,\text{rad}$ respectively, we retrieved the z and R data points generated by our simulation for droplets with a density ratio of 0.9. Figure 16 shows the experimental and numerical results graphed on the same axes. From these two data sets we were able to determine the difference in final drop height, contact angle, and volume.

Straight from the data points, we found that the final drop height from our video analysis was 3.4 mm, while the numerical results for a droplet of the same initial radius and contact angle revealed a droplet height of 3.8 mm. Additionally, we saw that the final θ in our experiment was 0.62 rad, while the simulation produced a final θ of 0.03 rad. Finally, we calculated the total volume for both data sets by summing

the small volume change $\mathrm{d}V_s$ from each $\mathrm{d}z$ step,

$$V_{\text{final}} = \sum_{j=0}^{n} \pi R_j^2 (z_{j+1} - z_j), \tag{48}$$

where n is the total number of data points (R_j, z_j) for either the experimental or numerical results. We found that the simulation produced a frozen droplet that was greater in volume by 15%. Not only does our model incorrectly predict a spherical top (final $\theta \approx 0$), but it overestimates the size for the solidified water droplet.

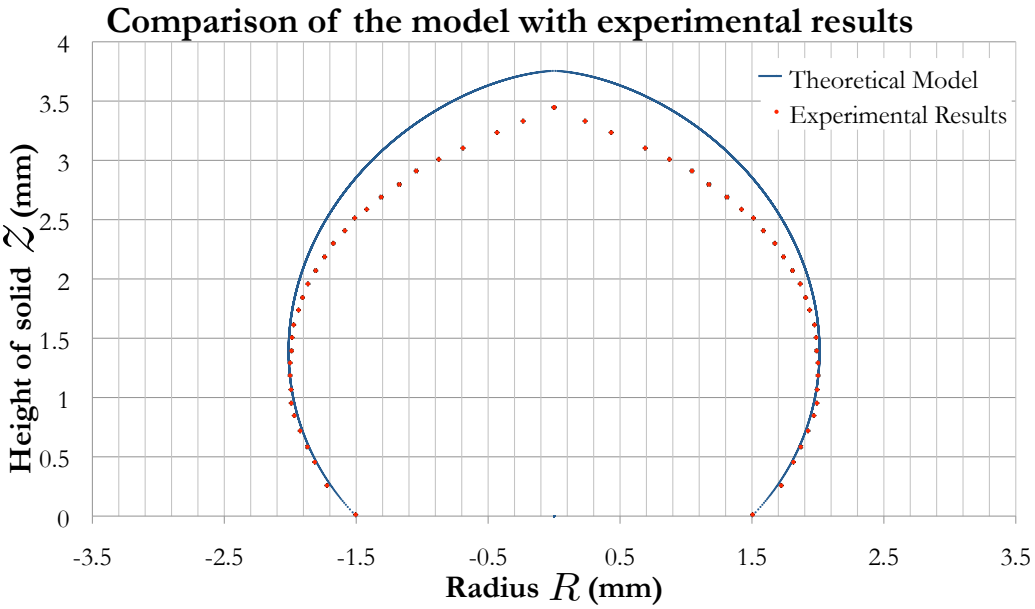

Figure 16: Graph of the frozen droplet dimensions as determined by our numerical results for $\nu = 0.9$ and compared with the experimental results. The data generated from our simulation was obtained such that it matched the $R_0 = 1.5\,mm$ and $\theta_0 = 2.29\,rad$ from our experiment.

4.2.2 Analyzing the differential equations

We used our *Ejs* program to create a graph of the final contact angle versus the density ratio, as seen in Fig. 17. By defining an event to store the resulting final contact angle for different ν, we ran the simulation over and over again, under the same initial conditions, while varying ν in small increments. From these collected values, we produced a graph similar to the positive quadrant of Fig. 4. Our program produced a flat-topped droplet for freezing liquids that have the same density in solid form ($\nu = 1$), and it predicted the appearance of a singularity for liquids that have

a density ratio less than about 0.78. This is slightly higher than the critical density ratio of 0.75 that we determined in Sec. 2.3.2.

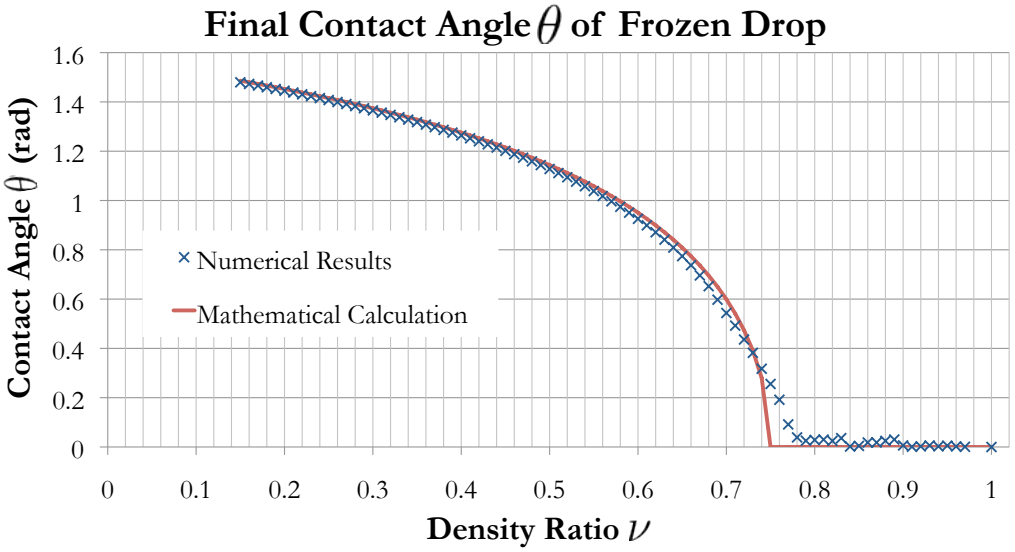

Figure 17: The final contact angle θ as a function of density ratio ν, generated by the numerical results of our Ejs simulation and the theoretical results of Eq. (46) (as seen in the positive quadrant of Fig. 4).

4.2.3 Creating an animation

We used our geometric model to produce a real-time animation of the freezing process by breaking down the solidifying drop into its liquid and solid portions. We generated an image at each time step, during which the computer program simulated the shape of the frozen half of the drop using the results for a density ratio $\nu = 0.9$ and the shape of the liquid portion using the results for $\nu = 1.0$ (corresponding to a flat-top, spherical cap shape). Since our *Ejs* program could not simultaneously handle the two components with their separate density ratios, we manually coded a new Java program to perform this task [11].

After collecting a series of frames of the intermediate droplet shapes, some of which are seen in Fig. 18, we used ImageJ [12] to create a GIF file. The animation runs on a loop for roughly 9.5 s, which was established based on the solidification rate equation with $\Delta T = 40\,\mathrm{K}$ and is a fairly accurate representation of our experimentally observed freezing times under these conditions. When played at the same time as our video (with the droplet freezing on an aluminum plate at about $T_c = -40\,^\circ\mathrm{C}$), the GIF runs slightly faster than the experimental solidification speed (see Fig. 19).

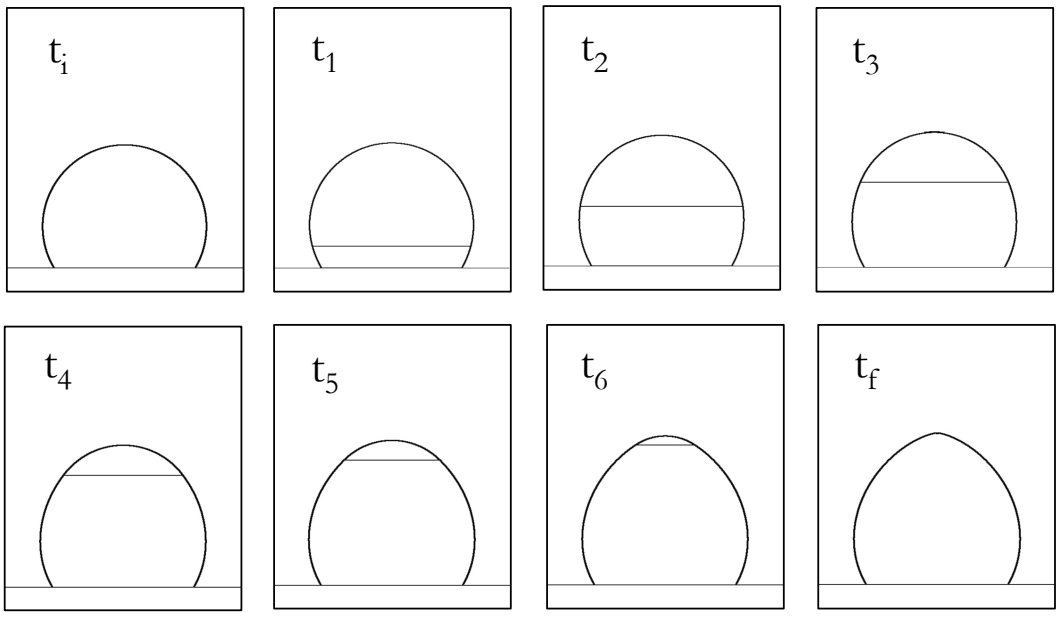

Figure 18: These images represent separate stages in a real-time animation of a water droplet transforming into a solid, rounded structure. Each frame was generated using our Java program [11] for a droplet with $\nu = 0.9$.

5 Discussion

Each of the two freezing methods had its own advantages and disadvantages. When we placed droplets directly on dry ice, they froze slower (probably because heat transfer is slower between water and dry ice versus the highly conductive metal plate). However, these videos are not as clear because there is a lot of frost and vapors flying around; additionally, the drop initially sinks down into the dry ice, which makes it difficult to immediately begin video analysis of the height of the solid. The temperature of the ice did remain at a constant -70 °C throughout our experiments.

The metal plate provided a uniformly-chilled, flat surface on which the droplets could freeze. However, the formation of frost and condensed vapor often changed the initial contact angle between the liquid and the plate if it was not completely cleared off. The temperature of the plate was constantly changing, either increasing or decreasing depending on whether the liquid Nitrogen was boiling away or when we added more to the polystyrene reservoir, respectively.

It makes sense that a density ratio of less than one would produce a conical drop. According to mass conservation, a solid volume being slightly larger than the liquid volume means the solid density must have been slightly smaller than that of the liquid. Furthermore, while the simplified model does predict the formation of singularities,

it does not accurately predict the shape of frozen water droplets, which have an approximate density ratio of 0.9. This can be seen in the quantitative comparison in Fig. 16 and the qualitative comparison in Fig. 19, where we overlay our experimental result with our numerical simulation. There is unfortunately a large gap between the experimental and our theoretically determined solid volume. This difference could be due to the neglect of some other parameter important to solidification, which may cause the radius and contact angle differential equations to approach zero too slowly.

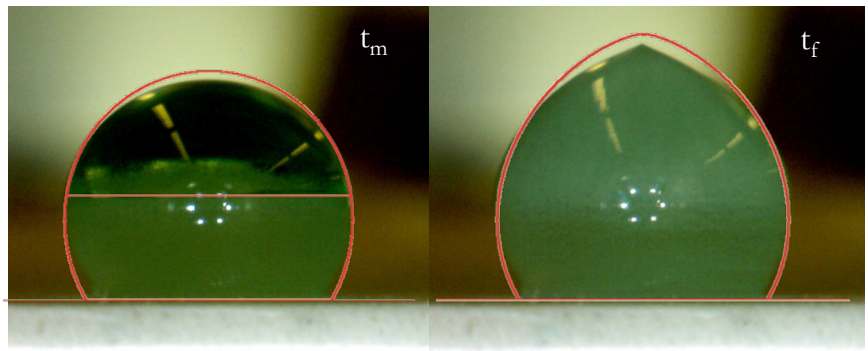

Figure 19: Screenshots from our experimental video (at a point t_m midway through and t_f at the end of solidification) compared with two frames from our animation (overlaid in red) generated by the simulation for a frozen water drop with $\nu = 0.9$ under the same initial conditions.

The solidification height graphs we determined from our experimental data (Figs. 9 and 11) roughly match the square-root behavior we expected from our theoretical Eq. (30) and its derivative. However, after plugging in the appropriate values, neither provides a sufficient fit to the data. The model appears to be most accurate for the first 3 s of drops freezing on a very cold aluminum plate (shown in Fig. 10). This could suggest that the one-dimensional temperature field is a fair approximation only during the initial moments of solidification.

It is also important to note that the $z(t)$ data for drops freezing directly on dry ice exhibit a unique behavior, as seen in the comparison with our theoretical model in Fig. 13. Our current model does not satisfy this, which means that our simplified way of looking at the thermal energy transfer within the solid portion of the drop cannot be applied to all types of freezing methods.

One final point of interest is the spontaneous quickening of the solidification rate at the end of the freezing process when the singularity appears. This is unfortunately something that cannot easily be studied from our videos, since the contact line becomes blurred towards the top of the drop. As seen from the larger error bars for the

data in the last second of solidification in Fig. 11, it is especially difficult to track the height of the solid layer in these final moments.

6 Modifying the theory

Previous research suggests the importance of taking a curved solid-liquid contact line into account for higher accuracy when modeling containerless solidification of sessile water droplets [13]. Specifically in one experimental video, a water droplet freezing directly on dry ice exhibits an unmistakably curved interface [6]. Figure 20 shows how the interface becomes increasingly curved as the drop solidifies.

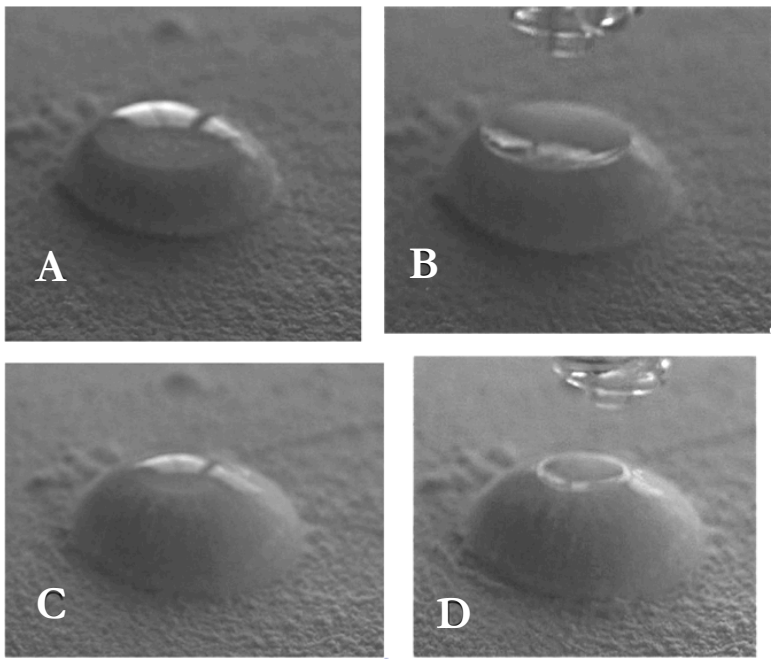

Figure 20: Photographs of the curved solid-liquid interface captured during previous research in this field [6]. A and C show the drop at two different points during solidification, whereas B and D show the solid portion of the drop after the liquid has been removed at the same respective points in time.

6.1 Curved Interface model

We looked briefly into the possibility of deriving a boundary-integral simulation, which would model the evolution of the three interfaces (solid-liquid, liquid-vapor, and solid-vapor) by means of the Green's function technique [14]. However, the complexity of this method appeared to be too involved for the limited amount of time we have for

our research. Despite that, it is possible to continue with a purely geometric approach for modeling this new parameter of the freezing process.

It is important to note that our solidification rate equation, Eq. (31), was derived from a one-dimensional temperature field assumption. However, because we are considering a curved contact line, we can no longer be sure that heat flux is independent of radius R. In fact, one might argue that the more complicated temperature gradient justifies a curved solid-liquid interface model. The more-isolated water molecules on the edges of the drop, which are colder, will lose thermal energy (and therefore freeze) faster. We therefore put aside our solidification rate equation and derive our radius, volume, and contact angle differential equations according to their dependence on the rising height z of the solid layer instead of time t.

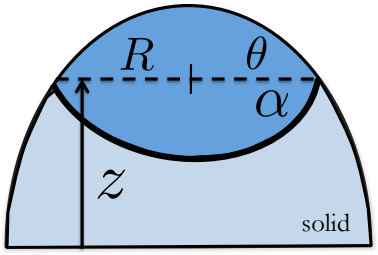

Figure 21: A diagram of the freezing droplet with a curved solid-liquid interface, which we attempt to model with an upside-down spherical cap. Note that we gain a new angle α, however our definitions for R, z, and θ are the same as in Fig. 1.

We illustrate this curve as if it is an upside-down spherical cap and define the same distances for z, R, and θ, as seen in Fig. 21. Hence, our changing radius is essentially the same as with our original model,

$$\frac{\mathrm{d}R}{\mathrm{d}z} = -\frac{1}{\tan\theta}. \tag{49}$$

Our liquid volume, changing volume, and changing contact angle equations are re-derived based on the new geometric configuration. Additionally, we define the new angle α of our upside-down spherical cap, as seen in Fig. 21.

Similar to our previous derivations of the spherical cap dimensions, we begin by constructing an equation for the radius of curvature $\mathcal{R}_c$ of the upside-down spherical cap (Fig. 22). To do so, we use the condition that the interface begins flat and then becomes increasingly spherical during solidification [13].

Our definition of $\mathcal{R}_c$ therefore has to include the conditions that at the beginning ($z = 0$) we should have a flat interface ($\mathcal{R}_c = \infty$), and when z approaches $z_{\max}$, $\mathcal{R}_c$ should approach R (which is approaching zero). One function that exhibits this

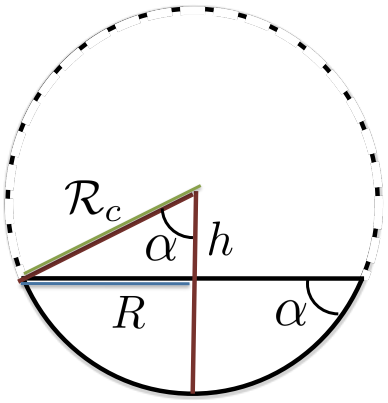

Figure 22: A representation of our upside-down spherical cap in the context of a complete sphere, used to derive the liquid volume and equation for α. Note, the radius of our spherical cap is still R, while $\mathcal{R}_c$ is the radius of the full sphere, and h is the height from the center of the sphere to the base of the cap.

behavior is

$$\mathcal{R}_c = R\ \mathrm{e}^{\beta(z_{\max}-z)/z}, \tag{50}$$

where $z_{\max}$ (corresponding to an approximate final drop height) and β (controlling how fast the interface becomes increasingly curved) are free-parameters that we adjust.

We use Eq. (50) and the geometry in Fig. 22 to find

$$\sin\alpha = \frac{R}{\mathcal{R}_c} = \mathrm{e}^{-\beta(z_{\max}-z)/z}. \tag{51}$$

Using Mathematica [15], we obtain the derivative of this equation with respect to z

$$\frac{\mathrm{d}\alpha}{\mathrm{d}z} = \frac{\beta z_{\max}\tan\alpha}{z^2}. \tag{52}$$

Similar to our original model, we look at mass conservation between the liquid and solid to derive a $\mathrm{d}V_l/\mathrm{d}z$ equation. The interface is curved, therefore we model the small interval volume of newly frozen solid as a spherical cap area A_{sc} with a thickness $\mathrm{d}\tau$, as shown in Fig. 23. We obtain the area of a spherical cap by integrating the circumference of a circle over a certain height, and putting this equation in terms of only R and α,

$$A_{sc} = 2\pi R^2\left(\frac{1}{1+\cos\alpha}\right). \tag{53}$$

Additionally, we derive an equation for the thickness of the solidification front $\mathrm{d}\tau$ in

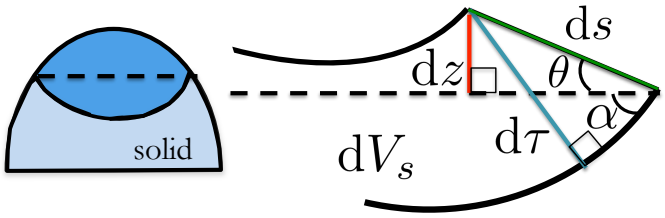

Figure 23: A zoomed in portion of the increasing dV_s slice, taking into consideration a curved solid-liquid contact line. The thickness of this segment is $d\tau$, whereas ds is the increasing length of the solid-vapor interface. The geometry presented here helps us derive Eq. (57).

terms of $\mathrm{d}z$ based on the geometry of the $\mathrm{d}V_s$ slice,

$$\mathrm{d}\tau = \sin(\theta+\alpha)\mathrm{d}s, \tag{54}$$

$$\frac{\mathrm{d}z}{\mathrm{d}s} = \sin\theta$$

$$\mathrm{d}\tau = \left(\frac{\sin(\theta+\alpha)}{\sin\theta}\right)\mathrm{d}z, \tag{55}$$

which really describes the $\mathrm{d}\tau$ and $\mathrm{d}z$ in terms of $\mathrm{d}t$. We can now use these relations to create an equation for $\mathrm{d}V_s/\mathrm{d}t = A_{sc}(\mathrm{d}\tau/\mathrm{d}t)$,

$$\frac{\mathrm{d}V_s}{\mathrm{d}t} = 2\pi R^2\left(\frac{1}{1+\cos\alpha}\right)\left(\frac{\sin(\theta+\alpha)}{\sin\theta}\right)\frac{\mathrm{d}z}{\mathrm{d}t}, \tag{56}$$

to substitute into Eq. (13). If we solve for $\mathrm{d}V_l/\mathrm{d}z$ and use our density ratio, we end up with

$$\frac{\mathrm{d}V_l}{\mathrm{d}z} = -\nu\ 2\pi R^2\left(\frac{1}{1+\cos\alpha}\right)\left(\frac{\sin(\theta+\alpha)}{\sin\theta}\right). \tag{57}$$

Using the same methods as mentioned in Sec. 2, our new total liquid volume (shown in Fig. 24) is simply going to be the original spherical cap volume (in terms of R and θ) plus the volume of our upside down spherical cap (in terms of R and α),

$$\begin{aligned} V_l(R,\theta,\alpha) &= V_{sc}(R,\theta) + V_{sc}(R,\alpha) \\ &= \frac{\pi R^3}{3}\left(\frac{2-3\cos\theta+\cos^3\theta}{\sin^3\theta} + \frac{2-3\cos\alpha+\cos^3\alpha}{\sin^3\alpha}\right). \end{aligned} \tag{58}$$

We finally derive an equation for the contact angle by taking the derivative of Eq. (58),

$$\frac{\mathrm{d}V_l}{\mathrm{d}z} = \frac{\partial V_l}{\partial R}\frac{\mathrm{d}R}{\mathrm{d}z} + \frac{\partial V_l}{\partial\theta}\frac{\mathrm{d}\theta}{\mathrm{d}z} + \frac{\partial V_l}{\partial\alpha}\frac{\mathrm{d}\alpha}{\mathrm{d}z}, \tag{59}$$

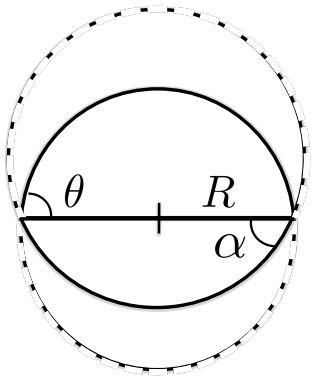

Figure 24: A representation of our total liquid volume, if we assume the freezing front is curved. Note our original spherical cap, with parameters R and θ, and the upside-down spherical cap, with parameters R and α. The relatives sizes of each sphere in this schematic are arbitrary.

solving for $\mathrm{d}\theta/\mathrm{d}z$, and plugging in each term that we know (see Appendix A.2) to get

$$\frac{\mathrm{d}\theta}{\mathrm{d}z} = \frac{4}{R}\cos^4\left(\frac{\theta}{2}\right)\left[1 - \frac{2\nu\,\sin(\theta+\alpha)}{(1+\cos\alpha)\,\sin\theta} - \frac{1}{4\,\cos^4(\theta/2)} + \frac{\tan\alpha}{\tan\theta} - \frac{(z^2 - R\beta z_{\max}\tan\theta)\tan\alpha}{4z^2\tan\theta\cos^4(\alpha/2)}\right], \tag{60}$$

where β and $z_{\max}$ are free-parameters, and α is defined as

$$\alpha = \sin^{-1}(\mathrm{e}^{-\beta(z_{\max}-z)/z}). \tag{61}$$

Using the equations for the changing radius R and contact angle θ, Eqs. (49) and (60) respectively, we should theoretically be able to predict frozen droplet shapes that are assumed to have a curved solid-liquid interface.

6.2 Experimental observations

Our goal was to either verify or disprove the curved interface in our own experiments. To do so, we used a regular-sized pipette to produce much larger water droplets (on the scale of mL), which we then froze by placing them directly onto dry ice. This freezing method was favored over using the cold plate apparatus, because droplets froze more slowly on the dry ice. Once the droplet was partially frozen, we used an empty pipette to quickly retract the remaining unfrozen liquid, in order to observe the shape of the freezing front. We repeated this process with several drops, taking away the unfrozen liquid at various points during solidification. While it was difficult to completely remove all of this liquid before the center started to freeze again, we

were able to observe the outer rim, which had a very slight curve. Overall, however, the drop appeared to have a relatively flat solid front, as shown in Fig. 25.

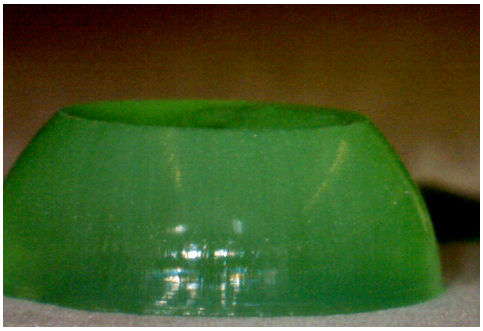

Figure 25: A photograph of a half-frozen water droplet from which we removed the top unfrozen liquid portion. The freezing front appears to be flat, which is inconsistent with our curved-interface theoretical approach.

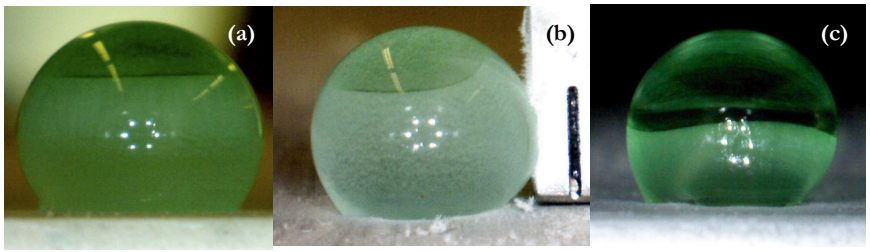

Figure 26: Series of images taken midway through the solidification of sessile water droplets. Note the differences in freezing front shapes between (a), (b), and (c).

Additionally, we present a few interesting examples of variously shaped freezing fronts that were observed: Fig. 26(a) has a very flat solid-liquid contact line, due to careful and even release of the drop onto the cold plate, Fig. 26(b) has an antisymmetric front due to a portion of the drop touching the cold metal ruler and therefore freezing faster on that side, and Fig. 26(c) has a lopsided solid-liquid interface, due one portion of the drop touching the cold plate and inadvertently starting to freeze before the liquid was completely released from the micropipette.

6.3 Numerical results

Taking a similar approach as with our Flat Interface model, we attempt to model a curved interface by updating our computer simulation with Eqs. (49), (60), and (61).

The graphical output we receive reveals that the simulation blows up after a certain point.

After breaking down the equation into parts, we have isolated a possible problem with the new $\mathrm{d}\theta/\mathrm{d}z$ equation, which contains our β free-parameter. For the purposes of troubleshooting, we made $z_{\max}$ very large such that it does not drastically effect our model. When $\beta = 1$ we see a highly flattened spherical drop, and when $\beta = 0.00001$ the sides of the drop vertically climb with no clear sign of convergence. However, when we attempt to use a value of β between these two extremes, we are seeing strange behavior that we are currently unable to explain.

6.4 Discussion

Theoretically, we believe our newly derived radius and contact angle differential equations are an accurate representation of how solidification would occur with a curved solid-liquid contact line. However when we insert these into our simulation, we are currently not seeing intelligible results.

Our experimental video of a water droplet freezing on our cold plate apparatus, taken at a perfectly horizontal angle, shows that the solid-liquid interface is very flat. We speculate that videos of solidifying sessile droplets showing a curved contact line contain this curve based on the initial conditions of the drop (for instance, the shape of the surface the drop is placed on, how carefully the drop is placed down, or the freezing method utilized).

It is important to note that the video from previous research exploring the contact line shape [6] shows the water droplet being dispensed into a small crater in the dry ice. This was presumably hollowed out to avoid the difficulties of having the liquid droplet slip off the piece of dry ice, which we described in our own experiment (Sec. 3.2). However, it is possible that this precaution was actually the cause of the formation of a curved interface. If the water droplet began solidifying in a spherical crater, it would inevitably cause the freezing front to take on the same shape.

Even without hollowing out a crater, when dropping water onto dry ice, it initially sinks down, inadvertently making the sides of the liquid drop near its base colder than the rest of the drop. Similarly, when freezing on the metal plate, the aluminum is so cold that it cools off the air directly above it, which means the sides of the liquid drop around the base are colder than other parts of the unfrozen drop. Thermal diffusivity is slightly dependent on temperature [16], therefore heat is transferred faster in these colder areas of the drop, translating to the sides of the drop beginning to freeze faster. This is also supported from the fact that we see various freezing front shapes (Fig. 26) based on which part of the water droplet touched a cold metal surface first.

Therefore, it may not be necessary to attempt to incorporate a curved interface into our geometric model.

7 Conclusion

Our research focused on analyzing freezing sessile water droplets; specifically we were interested in the singular tip that forms on the spherical liquid drops after solidification. Due to the volume of a solid drop with a pointy tip being greater than the volume of the original liquid sphere cap, the density of the solid has to be less than the density of the liquid in order for mass to be conserved. This phenomenon occurs for liquids that expand during freezing.

We created two purely geometric theoretical models to mathematically describe how the drops froze. Both models assume the unfrozen liquid begins in the shape of a spherical cap and that the slope of the solid layer equals that of the liquid layer during solidification. We derived a set of differential equations to describe how the volume, radius, and contact angle of the unfrozen liquid change with respect to the increasing $\mathrm{d}z$ of the solid front. We generated two computer programs to simulate the shape of the frozen droplet based on our two mathematical models.

The first model assumed that the solid-liquid interface is a flat line. This allowed us to theorize a simple, one-dimensional temperature field between the contact line and the plate, which gave rise to a solidification rate equation to describe how the height of the solid layer changed in time $\mathrm{d}t$. When we analyzed the stability of these equations, we determined that $\nu = 0.75$ is a critical density ratio, below which pointy drops will appear. The analysis helped us understand that even though a flat frozen drop with a final $\theta = 0$ is a solution for all ν, we will not see this in realty when $\nu < 0.75$ because small perturbations away from $\theta = 0$ result in the system evolving away from $\theta = 0$.

For our experiment, we built an apparatus that allowed us to observe small purified water droplets freezing on an aluminum plate, which was cooled from beneath by a liquid Nitrogen bath, as well as directly on dry ice. We recorded close-up videos of the solidification at various plate temperatures with a ProScope camera. We performed video analysis to obtain data on the R, θ, and z values at each time step. We looked at how the speed of the solid height changes with respect to the temperature difference between the cold plate and the freezing temperature, and found that the droplet freezes faster at colder plate temperatures, however it is difficult to draw conclusions from our analysis of droplets freezing on dry ice.

With the Flat Interface model, our computer program predicted the appearance

of the pointy tip for liquids with a density ratio less than 0.78, which was slightly higher than our theoretically determined critical ratio of 0.75. This program, however, did not accurately simulate the singularity which we experimentally observed for water droplets, with a density ratio of about 0.9. By comparing the experimental and numerical results, we found that the simulation predicts spherical frozen water droplets with about 15% larger volume than our observations.

Since our planar solid-liquid contact line model appeared incomplete, we considered a curved contact line, which had been described as being an important factor in previous research (see, for instance, Fig. 20).

In our second geometric model, we kept our differential equations in terms of $\mathrm{d}z$, since a curved contact line would mean there is probably a more complicated temperature field within the drop, and we therefore could not use our solidification rate equation. We did, however, derive a new equation to describe how the curve of the interface evolves during solidification. At this time, we are unfortunately unable to receive intelligible results from our program containing the Curved Interface model.

To experimentally investigate the shape of the solid-liquid contact line, we used much larger drops on dry ice, which froze slower, in order to remove portions of the unfrozen liquid sphere cap during solidification. At this time, we do not have conclusive evidence of a highly curved interface. The slight curve we observed could be due to the initial freezing conditions, and not necessarily an intrinsic property of droplet solidification.

This research helped us understand how the appearance of the singularity is dependent on the density ratio ν. We were able to both observe and create a general working model of this phenomenon. It began with reproducing a previously derived mathematical model [2], along with our own version of their experiment and simulation. We then expanded our work by drawing upon other research techniques [6] and theories [8]. Finally, we invented a new geometric model, which avoided the use of complicated boundary integral methods [13] [14], that was both valuable to and appropriate for an undergraduate level research project.

8 Suggestions for Further Research

It would be beneficial to revisit our derivation of the solidification rate. Our current model simplifies the situation by only looking at heat conduction within the frozen portion of the water droplet. However, we should be taking into account the cold surface that the drop sits on as being part of the system through which thermal energy is being transferred. There is definitely a difference between the thermal conductivity

of an aluminum plate and the thermal conductivity of dry ice, which could account for the difference we see between the $z(t)$ graphs for each freezing method.

Further research could investigate a mathematical model that considers the complicated tri-junction situation, as shown in Fig. 27. This model assumes that the slope of the solid layer does not equal the slope of the liquid layer during solidification, which means there is a growth angle between the two tangents. There is a subtle difference between the velocities of the liquid-vapor and solid-vapor interfaces, on the scale of μm/s [8], which may have an important role in determining the final drop profile. It would also be interesting to obtain experimental verification of the discontinuity in the slopes at the tri-junction. Our own experimental videos do not have a high enough resolution, and as of right now, there does not appear to be any photographs of this accepted phenomenon.

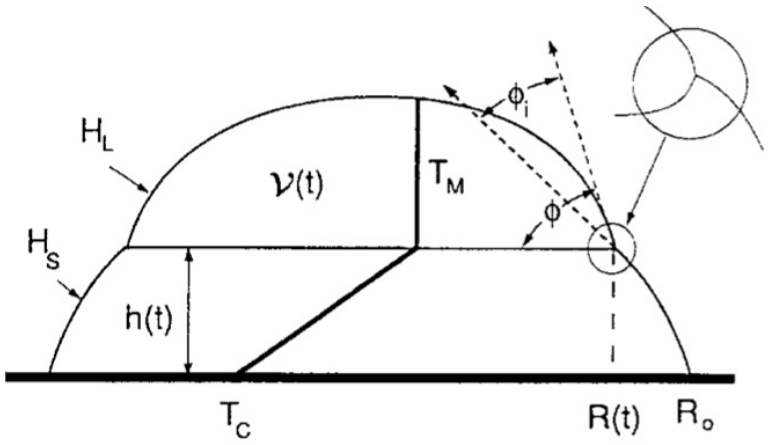

Figure 27: A diagram of the solidifying sessile water droplet that takes the complicated tri-junction into consideration. At the point where the solid, liquid, and vapor meet, the slope of the solid layer is slightly larger than the slope of the liquid layer, which gives rise to a growth angle ϕ_i between them. This angle is small and almost negligible at the beginning of solidification, and it gets much larger as the solid-liquid contact line approaches the top of the drop. [8]

A Deriving the contact angle differential equations

A.1 Flat Interface model

To derive how the contact angle θ changes with respect to the small height increment $\mathrm{d}z$, we must first start with differentiating our equation for the volume of a spherical

cap Eq. (11) with respect to z

$$\frac{\mathrm{d}V_l}{\mathrm{d}z} = \frac{\partial V_l}{\partial R}\frac{\mathrm{d}R}{\mathrm{d}z} + \frac{\partial V_l}{\partial \theta}\frac{\mathrm{d}\theta}{\mathrm{d}z}, \tag{62}$$

where the partial derivatives for V_l with respect to R and θ are

$$\frac{\partial V_l}{\partial R} = \pi R^2 \left(\frac{2 - 3\cos\theta + \cos^3\theta}{\sin^3\theta}\right) \tag{63}$$

$$\begin{aligned}\frac{\partial V_l}{\partial \theta} &= \frac{\pi R^3}{3}\left(\frac{\sin^3\theta(3\sin\theta + 3\cos^2\theta(-\sin\theta))}{\sin^6\theta}\right) - \left(\frac{(2 - 3\cos\theta + \cos^3\theta)(3\sin^2\theta\cos\theta)}{\sin^6\theta}\right) \\ &= \pi R^3\left(\frac{\sin^2\theta - \cos^2\theta\sin^2\theta - 2\cos\theta + 3\cos^2\theta - \cos^4\theta}{\sin^4\theta}\right).\end{aligned} \tag{64}$$

We solve Eq. (62) for $\mathrm{d}\theta/\mathrm{d}z$

$$\frac{\mathrm{d}\theta}{\mathrm{d}z} = \frac{\partial\theta}{\partial V_l}\left(\frac{\mathrm{d}V_l}{\mathrm{d}z} - \frac{\mathrm{d}R}{\mathrm{d}t}\frac{\partial V_l}{\partial R}\right), \tag{65}$$

and then substitute Eqs. (15), (17), (63), and (64) into this to end up with

$$\begin{aligned}\frac{\mathrm{d}\theta}{\mathrm{d}z} = \frac{1}{\pi R^3}&\left[\frac{\sin^4\theta}{\sin^2\theta - \cos^2\theta\sin^2\theta - 2\cos\theta + 3\cos^2\theta - \cos^4\theta}\right] \\ &\times \left[-\nu\pi R^2 - \left(\frac{-\cos\theta}{\sin\theta}\right)\left(\pi R^2\frac{2 - 3\cos\theta + \cos^3\theta}{\sin^3\theta}\right)\right]\end{aligned} \tag{66}$$

which simplifies to our differential equation for the shrinking contact angle [2]

$$\frac{\mathrm{d}\theta}{\mathrm{d}z} = -\frac{1}{R}[\nu - (1-\nu)(2\cos\theta + \cos^2\theta)]. \tag{67}$$

A.2 Curved Interface model

To derive how the contact angle θ changes with respect to the height of the solid front $\mathrm{d}z$, we must first start by differentiating our equation for the total volume of the liquid portion Eq. (58) with respect to z

$$\frac{\mathrm{d}V_l}{\mathrm{d}z} = \frac{\partial V_l}{\partial R}\frac{\mathrm{d}R}{\mathrm{d}z} + \frac{\partial V_l}{\partial \theta}\frac{\mathrm{d}\theta}{\mathrm{d}z} + \frac{\partial V_l}{\partial \alpha}\frac{\mathrm{d}\alpha}{\mathrm{d}z}, \tag{68}$$

which we solve for $\mathrm{d}\theta/\mathrm{d}z$

$$\frac{\mathrm{d}\theta}{\mathrm{d}z} = \frac{\partial\theta}{\partial V_l}\left[\frac{\mathrm{d}V_l}{\mathrm{d}z} - \frac{\partial V_l}{\partial R}\frac{\mathrm{d}R}{\mathrm{d}z} - \frac{\partial V_l}{\partial \alpha}\frac{\mathrm{d}\alpha}{\mathrm{d}z}\right]. \tag{69}$$

We have the partial derivatives $\partial V_l/\partial R$ Eq. (63) and $\partial\theta/\partial V_l$ Eq. (64) from Sec. A.1, and we can use a similar approach for the $\partial V_l/\partial\alpha$ partial derivative

$$\frac{\partial V_l}{\partial \alpha} = \pi R^3 \left(\frac{\sin^2\alpha - \cos^2\alpha \sin^2\alpha - 2\cos\alpha + 3\cos^2\alpha - \cos^4\alpha}{\sin^4\alpha} \right). \tag{70}$$

We substitute in our equations for $\mathrm{d}R/\mathrm{d}Z$ Eq. (17), $\mathrm{d}V_l/\mathrm{d}z$ Eq. (15), and $\mathrm{d}\alpha/\mathrm{d}z$ Eq. (52). After careful simplification, we finish with the following equation for the changing contact angle of a liquid drop freezing with a curved interface,

$$\frac{\mathrm{d}\theta}{\mathrm{d}z} = \frac{4}{R}\cos^4\left(\frac{\theta}{2}\right)\left[1 - \frac{2\nu\,\sin(\theta+\alpha)}{(1+\cos\alpha)\,\sin\theta} - \frac{1}{4\,\cos^4(\theta/2)} + \frac{\tan\alpha}{\tan\theta} - \frac{\tan\alpha(z^2 - R\beta z_{\max}\tan\theta)}{4z^2\tan\theta\cos^4(\alpha/2)}\right], \tag{71}$$

where α is defined as,

$$\alpha = \sin^{-1}(\mathrm{e}^{-\beta(Z_{\max}-z)/z}), \tag{72}$$

and β and $z_{\max}$ are free parameters.

References

[1] S. Strogatz, "Singular Sensations," *Opinionator*, The New York Times, (2012).

[2] J. H. Snoeijer and P. Brunet, *Pointy ice-drops: How water freezes into a singular shape*, Am. J. Phys. **80**, 764-771 (2012).

[3] K. Han and B. Michael, "Effects of Leading-Edge Ice Accretion Geometry on Airfoil Performance," *17th Applied Aerodynamics Conference*, Am. Inst. of Aeronautics and Astronautics, 379-390 (1999).

[4] Bodelin Technologies. Lake Oswego, Oregon. "*ProScope HR2*: Specifications." (2012).

[5] F. Esquembre, "*Easy Java Simulations*: The Manual." Ver. 3.4 (2005).

[6] M. Nauenberg, *Comment on "Pointy ice-drops: How water freezes into a singular shape"*, Am. J. Phys. **81**, 150-151 (2013).

[7] J. B. Fourier, *The Analytical Theory of Heat*. Trans. A. Freeman, (Dover Publishers, New York, 1955)

[8] D. M. Anderson, M. G. Worster, S. H. Davis, *The case for a dynamic contact angle in containerless solidification*, J. of Crystal Growth **163**, 329-338, (1996).

[9] Acknowledgements to L. English, Associate Professor of Physics at Dickinson College (*Carlisle, PA*), for help with the bifurcation and stability analysis (2013).

[10] Vernier Software and Technology. Beaverton, Oregon. "*LoggerPro*: Quick Reference." (2013).

[11] Acknowledgements to D. Lifschitz, Physics and Math major '13 at Dickinson College (*Carlisle, PA*), for coding the *Ejs* and Java programs (2013).

[12] T. Ferreira and W. Rasband, "*ImageJ*: User Guide." Ver. IJ 1.46r (2012).

[13] W. W. Schultz, M. G. Worster, D. M. Anderson, "Solidifying Sessile Water Droplets," *Interactive Dynamics of Convection and Solidification.* 209-226 (Kluwer Academic Publishers, The Netherlands, 2001).

[14] V. S. Ajaev and S. H. Davis, *Boundary-integral simulations of containerless solidification*, J. of Computational Phys. **187**, 492-503 (2003).

[15] S. Wolfram, "Wolfram *Mathematica* 9: Documentation Center." (2013).

[16] Ice - Thermal Properties, *Engineering Toolbox*, (1 Mar 2013) http://www.engineeringtoolbox.com/ice-thermal-properties-d_576.html.